GEOPHYSICS. VOL. 52. NO. 8 (AUGUST 1987); P. 1127–1137, 12 FIGS.

Airborne electromagnetic bathymetry

R. Zollinger*, H. F. Morrison*, P. G. Lazenby‡, and A. Becker*

ABSTRACT

Airborne electromagnetic techniques provide an efficient means for determining the bathymetry of shallow seas and coastal regions. Offshore time-domain data collected with the INPUT® system may be interpreted quickly and inexpensively using the simple table look-up algorithm described here. This interpretation algorithm is based on two dimensionless parameters which depend on the six channel amplitudes of the recorded INPUT data. These amplitudes are computed and tabulated for a suite of simple two-layer models in which seawater depth is the only variable quantity. The experimental data can then be interpreted by comparison with the tables of theoretical values to obtain the bathymetry beneath the flight path.

The inversion algorithm has proven accurate and stable. In the range of 0–40 m of seawater, the representative difference between the interpreted depths and the charted depths is about 2 m. Bottom gradients lower than 5 percent were resolved accurately beneath 0–25 m of water. Independent interpretations of data sets collected at different altitudes and in different directions show excellent repeatability. The algorithm exhibits low sensitivity to changes in the transmitter-receiver configuration and to variations in the underlying half-space conductivities when conductivity values are in the range 10^{-4}–10^{-1} S/m. The fractional error produced in the calculated depths by variations in the conductivity of the seawater is approximately equal to the fractional difference between the actual conductivity of the sea and the value of 4 S/m assumed in the model.

®Trademark of Barringer Research Ltd.

INTRODUCTION

Airborne electromagnetic (AEM) induction methods have been used for over 30 years to detect highly conductive metallic mineral deposits. Advances in modern solid-state technology and digital magnetic recording, however, have extended the use of AEM equipment to include the mapping of surficial formations. In this context, Dyck et al. (1974) interpreted time-domain AEM INPUT® data in terms of the thickness of the Champlain Sea clay formation near Hawkesbury, Ontario, Canada. Similar interpretations of frequency-domain AEM data in terms of conductive overburden thickness were published by Fraser (1978) and by Seigel and Pitcher (1978).

The use of airborne electromagnetics to determine the thickness of a surficial conductor was followed by the application of AEM methods to coastal bathymetry. This novel use of electromagnetics was first investigated by Morrison and Becker (1982), who concluded that most commercial AEM systems can be used for bathymetry investigations. Because of its low fundamental frequency, they suggested that optimal results could be obtained with the time-domain INPUT system. These predictions were subsequently verified in field tests by Zollinger et al. (1985) using time-domain INPUT data and by Won and Smits (1985) using frequency-domain DIGHEM data. This paper presents a simple data-interpretation scheme which facilitates the automatic interpretation of time-domain INPUT data in terms of the depth of the seawater. Because of its simplicity, the interpretation algorithm can be used for interpreting large amounts of airborne data quickly, inexpensively, and in real time.

®Trademark of Barringer Research Ltd.

THE INPUT SYSTEM

The INPUT® (INduced PUlse Transient) system was invented over 20 years ago by A. R. Barringer (1962) and has been

Presented at the 54th Annual International Meeting, Society of Exploration Geophysicists, Atlanta. Manuscript received by the Editor June 9, 1986; revised manuscript received December 22, 1986.
*Department of Materials Science and Mineral Engineering, University of California, Berkeley, CA 94720.
‡Questor Surveys Limited, Toronto, Ont., Canada.

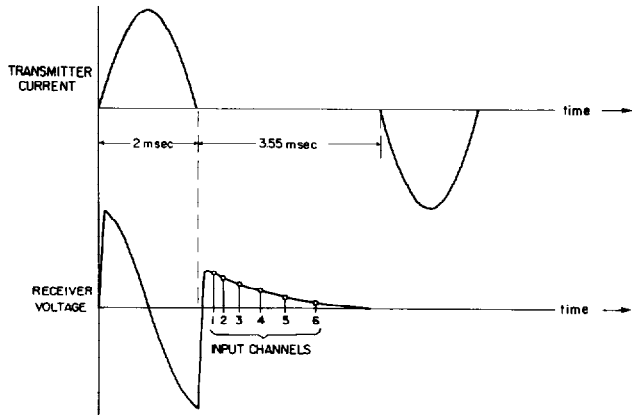

FIG. 1. The transmitter current waveform and corresponding receiver voltage for the INPUT system.

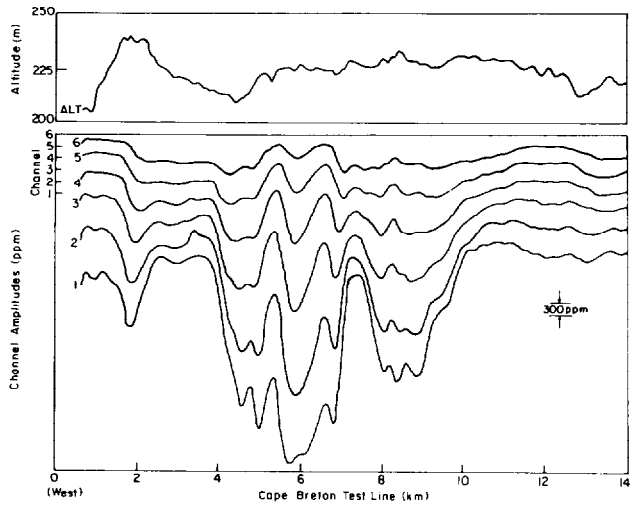

FIG. 2. A conventional INPUT record with compressed horizontal scale. The vertical scale is linear in parts per million and the zero level for each channel is offset 300 ppm as shown in the upper right corner of the record.

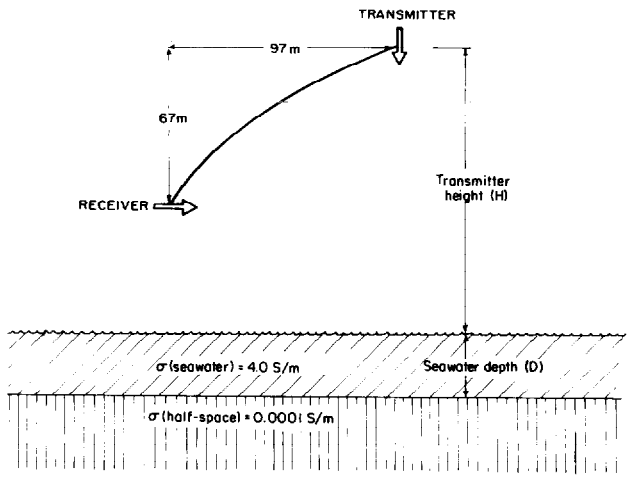

FIG. 3. Model parameters and INPUT system geometry.

modified a number of times since it was first operational. The INPUT MARK VI that is commercially available today has been described by P. G. Lazenby (1973). Briefly, this system consists of a vertical-axis magnetic-dipole transmitter which is rigidly attached to a fixed-wing aircraft and a horizontal-axis receiver located in a "bird" which is towed behind the airplane on 118 m of cable. At normal operating speeds (about 110 knots, 211 m/s), the receiver coil is located approximately 97 m behind and 67 m below the transmitter. In airborne bathymetry surveys, the transmitter uses a high-power 2 ms pulse to induce eddy currents in the water. After the transmitter is turned off, the receiver measures the secondary magnetic field produced by the decay of these eddy currents. The transmitted current and received voltage waveforms are shown in Figure 1. The secondary-field transient is sampled a number of times, beginning approximately 0.180 ms after the primary field is turned off. These samples are averaged within six time "windows" positioned along the transient. The six sample values (called "channels") represent the decay of the secondary magnetic field, and the time corresponding to each channel is taken as the center of the window. For the bathymetry tests, the six detector windows were centered at 0.28, 0.48, 0.78, 1.18, 1.68, and 2.28 ms after turnoff and were 0.2, 0.2, 0.4, 0.4, 0.6, and 0.6 ms wide, respectively. Because the INPUT process is repetitive, the results are stacked for about 1 s (180 repetitions of the primary pulse) to reduce noise. The final value of the observed secondary field within each of the windows is then recorded as a function of distance along the flight path. As shown in Figure 2, the observed data are displayed in parts per million of the peak amplitude of the primary field. For display clarity, the 0 ppm level for each channel is offset by a distance corresponding to 300 ppm from the zero level for the preceding channel.

INTERPRETATION OF INPUT DATA

The large amount of data collected in an AEM survey renders the use of classical inversion techniques, such as least-squares, prohibitively expensive and therefore impractical. Consequently, fast inversion schemes for time-domain data are often based on table look-up methods (Palacky and West, 1973; Dyck et al., 1974). In this type of scheme, the forward solutions for a suite of models are computed only once and stored for later use. The observed data at each point along the flight path are then compared with the stored theoretical data. The model parameters corresponding to the best-fitting theoretical data are then returned as the interpreted solution.

The interpretation algorithm we have developed is a fast, automatic curve-fitting routine, based on a simple two-layer model for analyzing offshore INPUT data. Shown in Figure 3, it represents conductive seawater covering a resistive bedrock so that in generating the theoretical INPUT data, only two parameters of the model are varied: the seawater depth D, and the height of the system above water H. The conductivity of the water is taken to be 4.0 S/m, and the underlying half-space is assumed to be almost infinitely resistive with a conductivity of 0.0001 S/m. The curve-fitting routine uses the INPUT data recorded during the survey along with the altimeter data to determine the one remaining model parameter, depth of the seawater.

Theoretical values for the horizontal component of the secondary magnetic field that would be detected by the INPUT system over the proposed model were calculated by using the familiar solution for the transient fields for a finite horizontal loop over a layered earth given by Morrison et al. (1969). The transient decay curves that would be measured by a system flying 230 m above a layer of seawater 0.5, 10, 30, and 100 m deep are shown in Figure 4. The amplitude of the transient is plotted logarithmically in parts per million of the peak primary field voltage measured at the receiver.

Modeling reveals that a slight change in the system's altitude, up to about 10 m, raises or lowers the amplitude of the whole transient without appreciably changing its shape, indicating that the rate of decay is independent of small variations in altitude. Altitude changes of more than 10 m, however, also produce changes in the transient decay rate, thereby affecting the relative amplitudes of the six INPUT channels. This indicates that any substantial changes in the aircraft's elevation must be taken into account by the interpretation algorithm so that altitude-induced variations in relative channel amplitude are not mistakenly interpreted as changes in seawater depth. Consequently, complete sets of theoretical decay curves were generated for a number of transmitter heights at 15 m intervals within the range of possible flight elevations. The field data were then interpreted by comparison with theoretical data calculated for a transmitter height within 7.5 m of the actual altitude of the aircraft.

Before fitting the field data to the theoretical curves, any overall shifts in the transient amplitude caused by small (< 10 m) altitude fluctuations or by slight changes in the relative positions of the transmitter and receiver ("bird swing") must be removed. The shifts are removed by dividing the amplitude of the transient at any given time by its amplitude at a fixed reference time, a normalizing procedure which does not affect the relative channel amplitudes. We have chosen to normalize the six-channel INPUT data by dividing each channel by the geometric mean amplitude of channels 3 and 4. These were selected as the normalizing channels because they are unlikely to become saturated if signal amplitudes are high, yet they maintain high signal-to-noise ratios when signal levels are low.

In Figure 5, the six theoretical, normalized channel amplitudes are displayed individually, showing the variation of each channel amplitude with increasing depth of seawater. Of course, channels 3 and 4 are distributed symmetrically about their geometric mean. An examination of Figure 5 reveals that for each seawater depth, the normalized transient may be described in terms of its early-time amplitude and the degree of symmetry of the six normalized channels about the 1.0 level. On this basis, the following two functions may be regarded as the characteristic quantities which (when used together) uniquely relate the six-channel INPUT data to seawater depth.

$$\text{Symmetry} = \text{SYM} = \sum_{i=1}^{6} \log \frac{\text{channel } (i)}{\sqrt{\text{Ch}(3)*\text{Ch}(4)}}, \qquad (1)$$

and

$$\text{Span} = \text{SPAN} = \sum_{i=1}^{3} \log \frac{\text{channel } (i)}{\sqrt{\text{Ch}(3)*\text{Ch}(4)}}. \qquad (2)$$

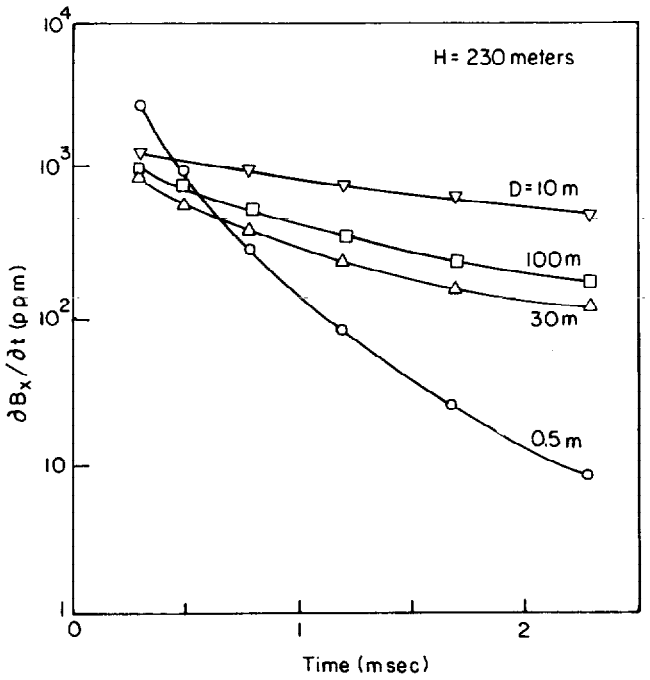

FIG. 4. Secondary-field transients observed at a flight altitude of 230 m above seawater which is 0.5, 10, 30, and 100 m deep.

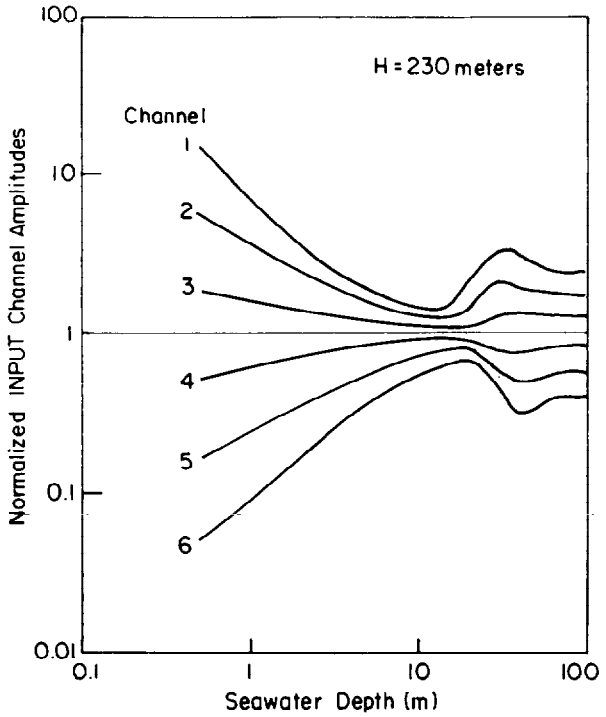

FIG. 5. The variation of channel amplitudes with the depth of seawater. These have been normalized by the geometric mean of channels 3 and 4.

SYM is the sum of the logarithms of all the normalized channel amplitudes and therefore characterizes the symmetry of the curves about the 1.0 level. In Figure 6, SYM = $a + b + c + d + e + f$. Notice that the logarithms of channels 4, 5 and 6 are negative, and that the contribution of channel 3 to the SYM function is canceled by that of channel 4. SYM, therefore, depends only on four channels: channels 1, 2, 5, and 6. SPAN is the sum of the logarithms of channels 1–3 and characterizes the early-time amplitude of the normalized transient. In Figure 6, SPAN = $a + b + c$. Figure 7 shows how SYM and SPAN change as the seawater depth increases from 0.5 to 100 m for a transmitter height of 230 m. These two characteristic variables may be used to interpret offshore INPUT data. Additionally, since they are generated by summing all or part of the observed data, SYM and SPAN contain proportionately lower levels of random noise than the individual channels.

In the tables used by the computer algorithm to analyze offshore INPUT data, the values of SYM and SPAN are stored at 1 m intervals over the depth range of 3–40 m. For shallower water the interval is reduced to 0.2–0.5 m, and in deeper water it is increased to 2–10 m. For each data point along the flight line, the automatic interpretation algorithm calculates SYM and SPAN from the six channels of INPUT data, selects the correct table of theoretical data based on the altitude of the aircraft, selects the correct region of the table based on SYM and SPAN, and then compares the two observed values of the characteristic quantities to each of fifteen theoretical pairs of such values that lie within the selected region. The algorithm returns the seawater depth which corresponds to the best-fitting pair. This "table lookup" process is carried out quickly and inexpensively, at a rate of about 0.002 CPU seconds per data point (a cost of about $0.05/mile or $0.05/105 data points) on a CDC 7600 mainframe computer.

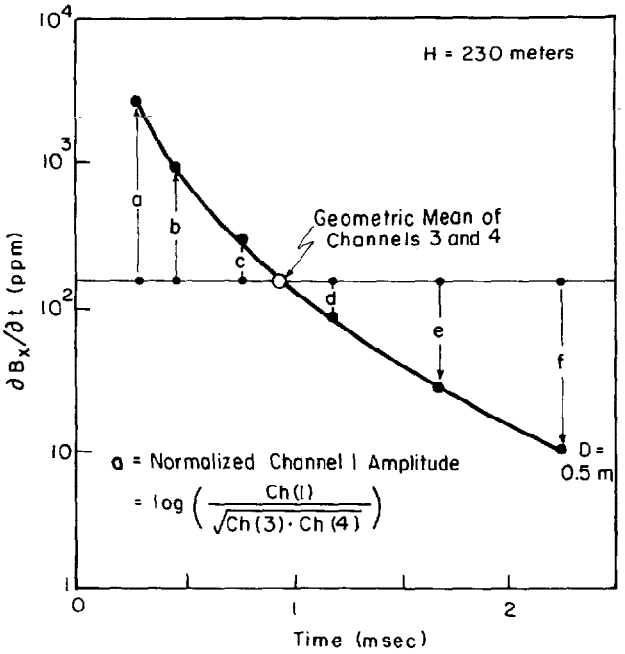

FIG. 6. Normalized secondary-field transient at a height of 230 m above 0.5 m of seawater. The geometric mean amplitude of channels 3 and 4 is indicated by the open circle.

FIELD EXAMPLES

Nova Scotia

The interpretation scheme developed in this investigation was first tested on 100 miles of offshore INPUT data collected during six flights along a single 17 mile long line which crosses the mouth of Lennox Passage near Cape Breton Island in Nova Scotia, Canada. The line was flown both east and west on a collinear track at altitudes of 170, 200, and 230 m (550, 650, and 750 ft) above sea level. Detailed bathymetry along the line, which is centered at 45°35'N, 60°50'W and runs N86°W, is available on Canadian Coastal Charts no. 4308 (scale 1 :37 500), no. 4275 (scale 1 :20 000), and no. 4279 (scale 1 :60 000).

The data collected while flying east at an altitude of approximately 230 m are displayed logarithmically in Figure 8. These data were acquired at a rate of 2 points/s, corresponding to a spatial interval of about 25 m. The channel amplitudes were then smoothed with a five-point weighted averaging filter, and the six channels were normalized by the geometric mean of the amplitudes for channels 3 and 4. Note that the west half of this record corresponds to the conventional INPUT record shown in Figure 2. In order to demonstrate their use in interpreting the data in terms of seawater

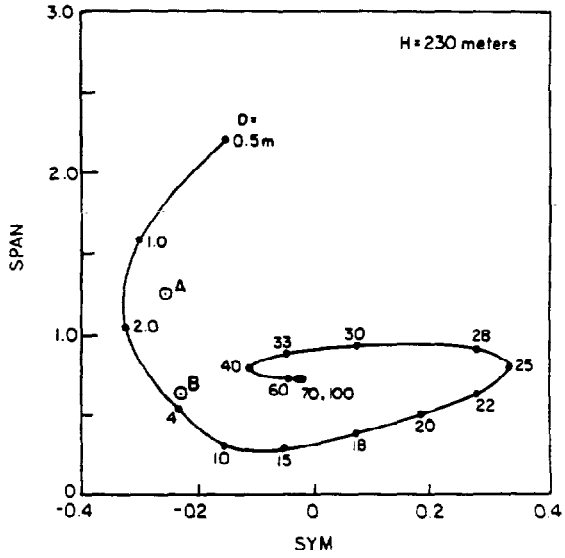

FIG. 7. The variation of the SYM and SPAN parameters as the seawater depth increases from 0.5 to 100 m.

depth, the SYM and SPAN values computed at two locations, A and B (shown in Figure 8), are plotted in Figure 7. This is the appropriate interpretation chart for the corresponding altimeter reading of approximately 230 ± 2 m. It indicates that the seawater depths at points A and B are 1.0 ± 2 m and 4.0 ± 2 m, respectively.

The results obtained with the six-channel interpretation algorithm for this data set are shown in the lower portion of Figure 8 where the interpreted depth profile is plotted with the corresponding known depth points taken from the appropriate coastal charts. These results were smoothed again with a running five-point averaging filter and obvious one- and two-point spikes removed. A deep, narrow anomaly at 12 km corresponds to the Lennox Passage. Here, the interpretation algorithm returns depths of 60–100 m for this feature, while the coastal charts indicate a maximum depth of 43 m. This range of depths corresponds to a very short segment of the curve in Figure 7, supporting the conclusions of Morrison and Becker (1982) that the ability of the INPUT system to resolve seawater depth is greatly reduced when depths exceed about 40 m. On the average, the depths interpreted from the INPUT data are within 2 m of the values taken from coastal charts. However, this comparison does not provide a good measure of the accuracy of the interpretation algorithm due to inaccuracies in the coastal depth sounding measurements, location errors, and changes in seawater depths related to daily tide and yearly sedimentation cycles.

To evaluate the accuracy of this data-interpretation method, the results of four different traverses along the same flight line are shown in Figure 9. Lines 13E and 14W were flown at 230 m and lines 15E and 16W were flown at 200 m above sea level (E and W indicate the direction flown). It is encouraging to note that the individual interpretations for each of the four data sets agree to within 2 m of the average interpreted depth value in most parts of the surveyed line.

New Brunswick

One other set of offshore INPUT data was used in a second test of the interpretation algorithm. These data were collected during four traverses along a single, 19 km line which crosses Savoy Landing and Pokesudie Island in New Brunswick, Canada. The flight line, beginning at 47°45′N, 64°39.5′W and bearing N50°W, extends over deep water on the northwest end. Of the four data sets collected, two were recorded outbound (beginning over land and ending about 16 km off the coast) and two were recorded inbound. Only the outbound lines (1NW and 3NW) were interpreted, since these were easily located on a map while using visual flight-path navigation.

This data set was acquired at a relatively high altitude in the range of 210–240 m so that the signal level in the last two channels was too low to be of any value in the interpretation procedure. Consequently, the signal level was interpreted using a modification of the six-channel procedure just described. Details of the modified interpretation procedure are given by Zollinger (1985).

The first four normalized channels of INPUT data collected on an outbound flight (line 3NW) and the compiled interpretations for lines 1NW and 3NW are shown in Figure 10. Both the data and the interpreted depth profile have been smoothed with a five-point averaging filter. The seawater depths, known or inferred from Coastal Chart no. 4439, are also plotted for comparison with the interpreted values. While the overall fit is reasonably good, there are a few places, especially on line 1NW, where the data were not interpreted correctly. The misinterpretation occurs most often when the seawater is 7–17 m deep and the observed transients are very flat. In this case, as exemplified by the transient for 10 m of water shown in Figure 4, the data are very sensitive to noise. Transients in this depth range have somewhat different overall amplitudes before normalization, but their early-time decay rates are virtually identical. Thus, as may be seen in Figure 5, the normalized transients are the same for channels 1–3, and minor noise in channel 4 may cause the transient over 7 m of water to be mistaken for a transient over 17 m of water. The result is the type of excursion seen in the interpreted depth profile for line 1NW at 15, 18, 20, and 21 km along the flight line.

As the water depth begins to increase at about 24 km along the profile, it appears that the INPUT data, even for the low signal levels measured at transmitter altitudes greater than 200 m, can be interpreted for seawater shallower than 50 m. Some difficulty is then encountered in attempting to resolve the gradient between 25.5 and 26 km, but a good estimate of depth is returned when the bottom levels out at about 40 m, between 26 and 28 km. To illustrate, the data and depth interpretations for line 3NW from 22–26.5 km are displayed in Figure 11 on an expanded scale. The theoretical data for the water depths given by the coastal charts are also shown in order to demonstrate how sensitive the four-channel interpretation is even to a small amount of noise in one of the channels. Because the signal levels at an altitude of 200 m over moderately deep water are quite low (channel 4 amplitude values are 200–300 ppm), normal survey noise levels of up to 40 ppm could result in the type of errors indicated on this profile.

ERROR ANALYSIS

The observed differences between the bathymetry interpreted from the INPUT data and that extracted from the coastal charts may be quantified in three ways. First consider the average error, which is the sum of all the errors, positive and negative, divided by the number of points where it was calculated. This quantity should approach zero if the errors are random. Another measure is the average absolute error, sometimes called the mean deviation, which is the sum of the absolute values of the observed errors divided by the number of points. Finally, we consider the root-mean-square (rms) error, which is essentially the standard deviation of the errors from zero when the errors are distributed normally. In the field cases studied, however, no claim can be made for a normal population distribution, so the rms error does not exhibit the statistical properties normally associated with standard deviations. It does, however, give some indication of the scatter in the data.

The following errors were calculated for the four lines of data flown in Nova Scotia (lines 13E, 14W, 15E, and 16W) and for the two outbound lines flown in New Brunswick

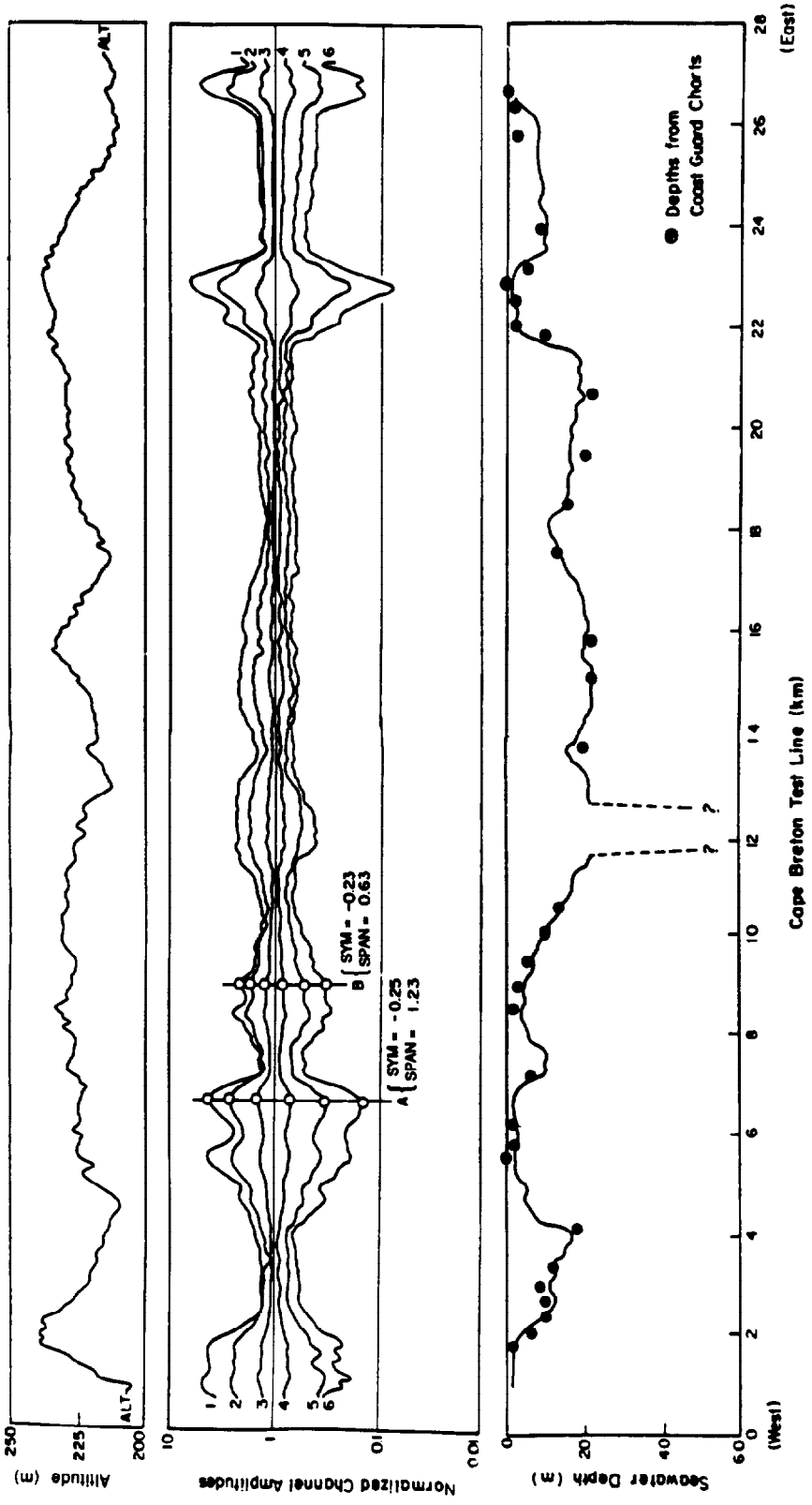

FIG. 8. Interpreted INPUT data from Nova Scotia with the corresponding bathymetry from coastal charts.

(lines 1NW and 3NW).

	L13E	L14W	L15E	L16W	L1NW	L3NW
Average error (m)	0.41	−0.27	0.32	0.00	−0.36	0.12
Average absolute error (m)	2.32	2.05	2.19	2.38	1.40	1.58
Root-mean-square error (m)	3.07	2.54	2.97	2.92	2.02	1.85

A number of possible sources of error were investigated to explain the observed discrepancies between the interpreted bathymetric profiles and the bathymetry values on the charts. Of these, the principal sources of error appear to be:

(1) noise in the data which is caused by atmospherics or by the motion of the receiver coil through the Earth's magnetic field;

(2) variations in the position of the receiver coil with respect to the transmitter and the surface of the seawater; and

(3) the effects of basing the interpretation algorithm on an inadequate model. For example, the seabottom is not always highly resistive and the seawater does not have a constant conductivity of 4.0 S/m.

Three additional sources of error which were not investigated quantitatively, but which may play a significant role, are errors in the aircraft position, inaccuracies in coastal charts due to seasonal changes in seabottom topography, and use of a one-dimensional algorithm to interpret three-dimensional seabottom features. While the effects of three-dimensional features were not examined, satisfactory results over fairly steep gradients were obtained in Nova Scotia and to a lesser extent in New Brunswick. Thus it appears that the highly conductive seawater rapidly attenuates EM fields away from the transmitter, diminishing the effects of lateral changes in seabottom topography.

System noise

This source of error was investigated by adding known amounts of random noise to theoretical data before interpreting them with the standard six-channel algorithm. Fifty trials were done at each noise level in order to obtain a statistically valid estimate of the error.The results of these tests show that even with the addition of 50 ppm of noise, reasonably good bathymetric estimates can be made for seawater depths up to nearly 30 m. These estimates show an average absolute error of about 2 m and an rms error of about 3 m. If the system noise is reduced to 20 ppm, the interpretation algorithm resolves the seawater depth within 1 m for depths up to 40 m. Under normal survey conditions, the INPUT system has a noise level of about 30 ppm, but noise levels as low as 10 ppm have been achieved under optimal conditions.

Changes in transmitter-receiver configuration

Because the receiver is towed behind the aircraft on 118 m of cable, its actual position is dependent upon the speed of the aircraft, wind, and turbulence. Unrecorded and irregular changes in the system configuration, often called "bird swing," can cause errors in interpretation because the algorithm is set up for a receiver located 97 m behind and 67 m below the aircraft. In this position, it is towed at an angle of about 35 degrees below the horizontal plane defined by the transmitter. Nevertheless, most of the effects introduced by the receiver's deviations from this equilibrium position are removed by the normalization process. A detailed analysis of this problem shows that variations in tow angle of ± 5 degrees from the normal value result in bathymetric errors of less than 1 m. Errors introduced by variations in the bird's pitch and yaw were not studied in this investigation.

An inadequate model

Variation in seawater conductivity.—The conductivity of seawater depends on temperature, salinity, and pressure. Both temperature and salinity are highly variable in shallow seas and coastal areas. Consequently, the conductivity of the top 100 m of seawater can range from 5.5 S/m in equatorial areas to 3.2 S/m in polar regions (Bullard and Parker, 1970). In general, 4.0 S/m is a good first estimate of the conductivity of shallow seawater at 45°N latitude. Won and Smits (1985) made eight spot conductivity measurements in Cape Cod Bay (~42°N latitude) which fell in the range 4.0–4.12 S/m. However, decreases in salinity due to the influx of fresh water or increases in salinity because of barriers which prevent seawater mixing, and higher temperatures in very shallow areas, can all cause heterogeneity in the conductive water layer.

Because the interpretation algorithm contains a constant seawater conductivity of 4 S/m, any changes in the conductance of the water layer will be interpreted as changes in water depth. Thus, if the actual seawater conductivity is 3.6 S/m (10 percent lower than the assumed value of 4 S/m), the interpreted water depth will be 10 percent lower than its true value.

Variation in sea-bottom conductivity.—The effects of assuming a 0.1 S/m half-space were investigated by calculating theoretical secondary-field transients for a number of two-layer models where the depth of the seawater and the conductivity of the sea bottom were varied. These transients were then interpreted with the standard algorithm which assumes the bottom to be highly resistive. The results of these calculations are presented in Figure 12, which shows that sea-bottom conductivities up to 100 mS/m introduce no more than 1 m of error in the depth estimates. When the sea-bottom conductivity increases to 1 S/m, the method fails for very shallow and for very deep water. As it fails, erratic depth estimates are returned, thus indicating that the interpretation algorithm is no longer operating properly.

In a related study, Turnross (1984) examined the feasibility of using AEM methods to map the resistivity of a thin, conducting layer placed on an otherwise resistive sea floor. Using a Levenburg-Marquart least-squares algorithm to invert theoretical INPUT data, she concluded that the errors in estimates

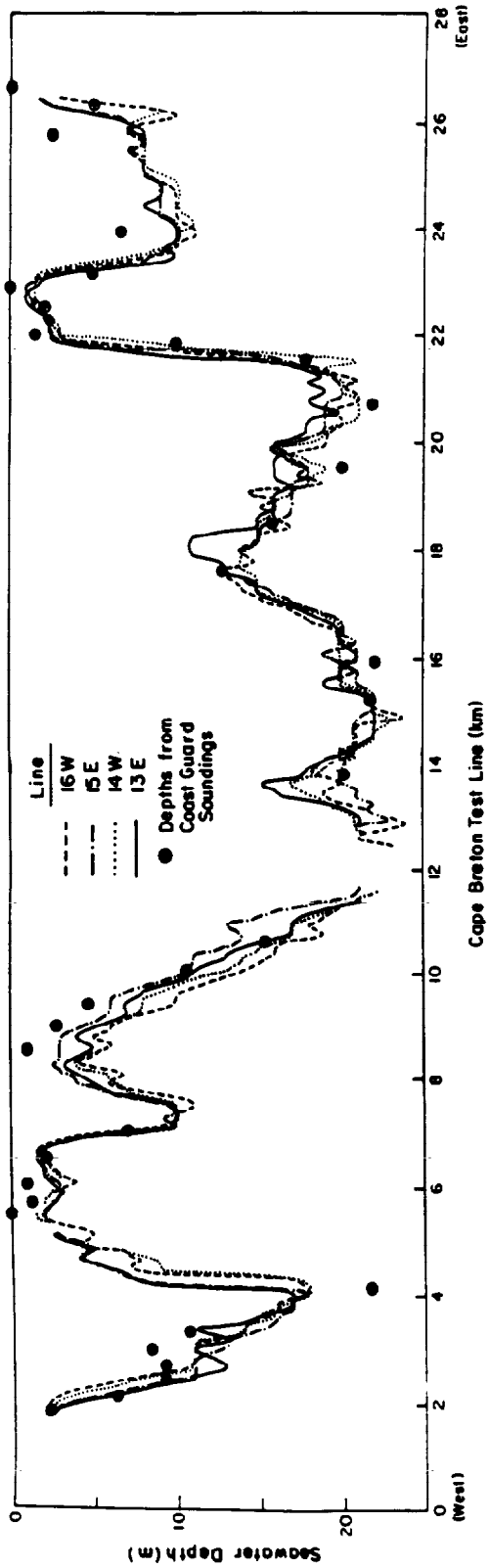

FIG. 9. A compilation of the results of interpreting four different INPUT data sets collected along the same line in Nova Scotia.

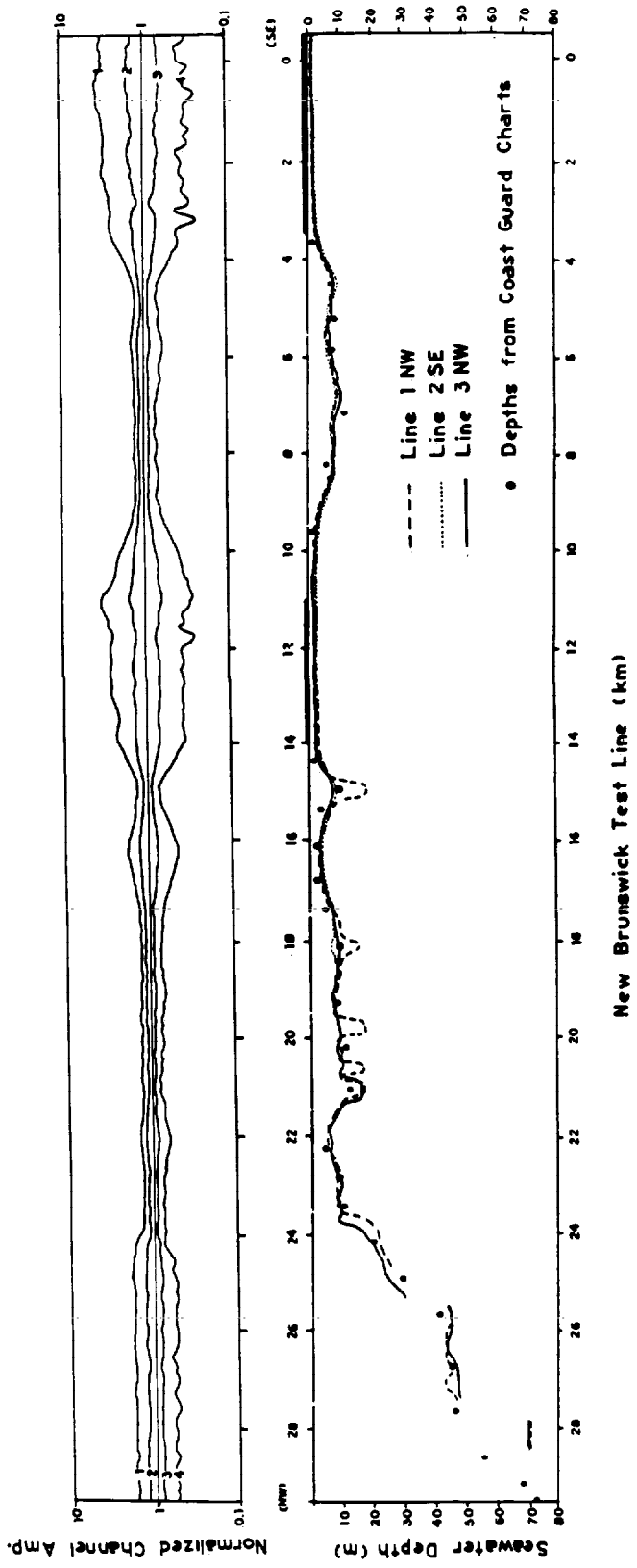

FIG. 10. INPUT data and the compiled seawater depth interpretation along a line in New Brunswick, Canada.

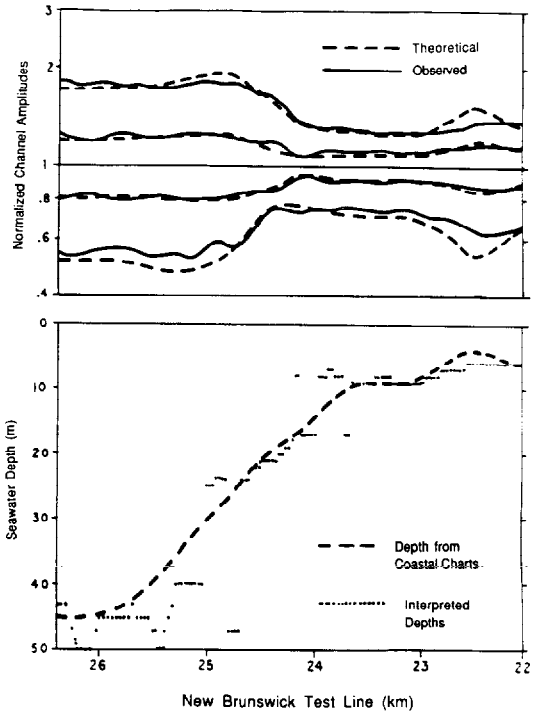

FIG. 11. The observed INPUT data over deepening water along the New Brunswick test line are plotted on an expanded scale along with the theoretical INPUT data generated using coastal bathymetry (top). The theoretical data were generated for an aircraft elevation of 210 m, water conductivity of 4.0 S/m, and an underlying half-space conductivity of .1 mS/m. The interpreted depths and the depths from coastal charts are shown on the bottom graph.

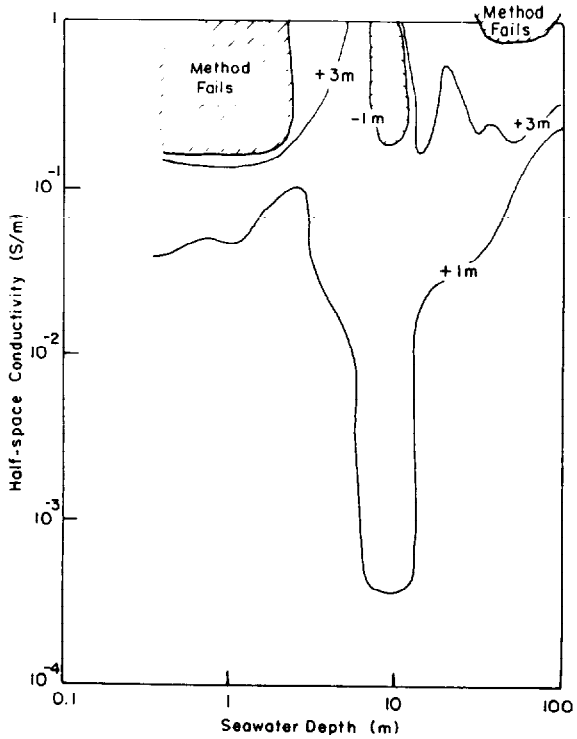

FIG. 12. The error introduced by changing the half-space conductivity as a function of the depth of the seawater.

of the water depth caused by ignoring the presence of a thin layer of conducting bottom sediments were similar to those due to an improper estimate of the conductivity of seawater. Because our interpretation algorithm correctly estimates the total conductance of the seawater and the bottom sediments, we expect that the omission of this layer will result in an overestimation of seawater depth by an amount roughly equal to the ratio of the sediment conductance to the seawater conductance.

We have not attempted to develop a three-layer algorithm which interprets sediment thickness and conductivity because the complexity of such a scheme would not likely allow for the processing speed necessary in the routine application of this method to airborne bathymetric surveys. Many standard inversion packages, such as the one used by Turnross (1984), can invert the data in terms of the conductivity and the thickness of several layers. These inversions typically can take 10–100 times as much computer time as is required by the simple scheme presented here to interpret each data point.

CONCLUSIONS

Using a simple two-layer model, it is possible to interpret offshore INPUT data in terms of the depth of the seawater quickly, inexpensively, and accurately. Test cases show that in the range of 0–40 m of seawater, the representative difference between the interpreted depths and the charted depths recorded by traditional bathymetric soundings is about 2 m. Bottom gradients up to 4 percent under 0–25 m of water were resolved accurately, and independent interpretations of data sets collected at different altitudes and in different directions show excellent repeatability. The inversion algorithm is very stable, being little affected by system noise and variations in system geometry when the water is less than 30–40 m deep. As implied by the test results, the errors caused by neglecting small changes in seawater conductivity, sea-bottom conductivity, and the presence of sea-bottom sediments affect the accuracy of the interpreted depths by about ± 2 m. Because the simplicity of the algorithm was a key objective, no attempt was made to interpret the data in terms of seawater conductivity and the conductivity of the bottom sediments. This additional interpretation can be done using a more complex algorithm for interpreting INPUT data, such as the two-tier table look-up scheme presented by DeMoully and Becker (1984) or the least-squares inversion algorithm used by Turnross (1984). As the equipment is upgraded (Lazenby and Becker, 1986), the simple algorithm presented here will have to be modified to take advantage of the improved data. In the meantime, it can be used effectively to obtain fairly accurate bathymetric estimates using conventional MARK VI data.

ACKNOWLEDGMENTS

This work was funded in part by NORDA under contract no. N00014-84-K-0556.

REFERENCES

Barringer, A. R., 1962, The INPUT electrical pulse prospecting system: Min. Cong. J., **48**, 49–52.

Bullard, E. C., and Parker, R. L., 1970, Electromagnetic induction in the oceans, *in* Maxwell, A. E., Ed., *The Sea*, **4**, Wiley-Interscience, 695–730.
DeMoully, G. T. and Becker, A., 1984, Automated interpretation of airborne electromagnetic data: Geophysics, **49**, 1301–1312.
Dyck, A. V., Becker, A., and Collett, L. S., 1974, Surficial conductivity mapping with the airborne INPUT system: CIM Bull., **67**, 104–109.
Fraser, D. C., 1978, Resistivity mapping with an airborne multicoil electromagnetic system: Geophysics, **43**, 142–172.
Lazenby, P. G., 1973, New developments in the INPUT airborne EM system: CIM Bull., **66**, 96–104.
Lazenby, P. G., and Becker, A., 1986, Redefinition of the INPUT system: Ontario Geol. Surv., open-file rep. 5609, 1–32.
Morrison, H. F., Phillips, R. J., and O'Brien, D. P., 1969, Quantitative interpretation of transient electromagnetic fields over a layered half space: Geophys. Prosp., **17**, 82–101.
Morrison, H. F., and Becker, A., 1982, Analysis of airborne electromagnetic systems for mapping depth of seawater: Final report, ONR contract no. N00014-92-M-0073.
Palacky, G. J., and West, G. F., 1973, Quantitative interpretation of INPUT AEM measurements: Geophysics, **38**, 1145–1158.
Seigel, H. O., and Pitcher, D. H., 1978, Mapping earth conductivities using a multi-frequency airborne electromagnetic system: Geophysics, **43**, 563–575.
Turnross, J., 1984, Analysis of airborne EM systems for mapping conductivity and thickness of bottom sediments: M.Sc. thesis, Univ. of California, Berkeley.
Won, I. J., and Smits, K., 1985, Determination of electrical depths and bottom characteristics of shallow oceans using the airborne electromagnetic method: NORDA rep. 106.
Zollinger, R., 1985, Airborne electromagnetic bathymetry: M.Sc. thesis, Univ. of California, Berkeley.
Zollinger, R., Becker, A., and Morrison, H. F., 1985, Data analysis for airborne electromagnetic bathymetry: NORDA rep. 93.